J. Phys. B: At. Mol. Opt. Phys. 26 (1993) 3147–3158. Printed in the UK

Elastic and vibrationally inelastic cross sections and energy loss spectra for electron collisions with GeH_4*

M A Dillon, L Boesten†, H Tanaka†, M Kimura and H Sato‡
Argonne National Laboratory, Argonne, IL 60439, USA

Received 2 November 1992, in final form 19 February 1993

Abstract. Absolute vibrationally elastic cross sections for e-GeH_4 collisions have been determined for electrons of 1, 2, 2.5, 3, 5, 7.5, 10, 15, 20, 60 and 100 eV incidence energy over a scattering angular range of 10°–130°. The observed angular distributions correspond, at least qualitatively, to theoretical formulations using the continuum-multiple-scattering method, the parameter-free static-exchange-polarizaton approximation, and a multichannel Schwinger variational calculation. Vibrational excitation functions and the energy distribution of elastically scattered electrons reveal a shape resonance at about 2–2.5 eV. Calculations show that the resonance scattering state belongs to the t_2 representation of the T_d point group, which is also the representation of the *lowest unoccupied molecular orbital* (LUMO) of GeH_4.

Energy loss spectra recorded in the electronic threshold region of GeH_4 reveal enhanced inelastic scattering at large angles in the loss range 7–9 eV characteristic of excitation to the lowest triplet state.

1. Introduction

Because of their prominence in the field of chemical plasmas, CH_4 and SiH_4 have been the subject of extensive theoretical and experimental investigations involving electron collisions (Tanaka *et al* 1988, 1990b, Boesten and Tanaka 1991). On the other hand, the third of the group IV tetrahydrides, germane (GeH_4), has received scant attention even though it has considerable potential as a semiconductor reactant (see, e.g., Osmundsen *et al* 1985). More importantly, the relatively large mass of its centre makes germane an ideal testing ground for e-molecule collision and photoionization theories that rely on approximately spherically symmetric potentials. In this connection, e-GeH_4 scattering in the energy range 1–100 eV has already been investigated theoretically by Jain *et al* (1991) in a spherical field *static exchange polarization* (SEP) approximation. In addition, a formulation of the *multichannel Schwinger variational method* (MSV) has been used to characterize electron collisions with GeH_4 (Winstead and McKoy 1992).

After an outline of the experimental results, we describe in section 2.2 our implementation of the *continuum multiple scattering* (CMS) method to model the e-GeH_4

* Work supported in part by the US Department of Energy, Office of Energy Research, Office of Health and Environmental Research, under contract W-31-109-Eng-38.
† Present address: Departments of Physics and of General Sciences, Sophia University, Tokyo, Japan.
‡ Present address: Department of Physics, Ochanomizu University, Tokyo, Japan.

0953-4075/93/183147+12$07.50

scattering problem. In sections 3.1–3.3, we compare the results of the various theoretical approaches to measurements of the elastic differential and integral cross sections of GeH_4. Finally, as a supplement we add in sections 3.4–3.6 a limited range of measurements of vibrationally inelastic *electron energy loss spectra* (EELS), excitation functions and EELS in the electronic threshold region.

2. Techniques

2.1. Experimental techniques

The scattering apparatus and methods employed in this work have been amply documented in previous publications (Tanaka *et al* 1990b), so that only a brief summary is provided here. The spectrometer consists of a matched pair of hemispherical condensers, one serving as monochromator and the other as a rotatable energy analyser. Between the condensers, a beam of electrons of incidence energy 2–100 eV and resolution 40 meV intercepts a molecular beam of GeH_4 from an effusive jet at right angles. The scattered electrons are projected onto the focal plane of the energy analyser by means of a computer-controlled achromatic lens system (Boesten 1988). Differential pumping of both the monochromator and the energy analyser insures that a potentially deleterious gas like GeH_4 has a minimal effect on the electron optics. Cross sections were obtained by the relative flow method using helium as the comparison gas and a previously compiled cross section set (Boesten and Tanaka 1992). The incident energy was calibrated against the 19.37 eV resonance of helium. The energy scale for vibrational excitation functions and elastic scattering energy distributions was calibrated by reference to the 1.97 eV peak of N_2 ($v = 0 \rightarrow 1$) in an $N_2 + GeH_4$ mixture. The energy resolution (40 meV) is not sufficient to resolve the adjacent vibrational bands $\nu_1 \approx \nu_3$ (0.259, 0.262 eV) and $\nu_2 \approx \nu_4$ (0.116, 0.104 eV). These overlapping pairs correspond respectively to stretching and bending vibrations and are designated ν_s and ν_b in the remaining discussion. Experimental errors are estimated to be 15–20% for elastic differential cross sections and 30% for vibrational excitation cross sections.

2.2. Theoretical techniques

To aid the interpretation of our experimental results, we have calculated the e-GeH_4 elastic cross sections by using the well documented CMS method (Dill and Dehmer 1974, Kimura and Sato 1991). A brief exposition of its approach will suffice. To render the e-molecule collision problem tractable, the CMS method partitions configuration space into three contiguous and spherical regions: I, the atomic region; II, the interstitial region; and III, the asymptotic region. In the present application an approximate molecular Hartree–Fock wavefunction for the atomic region that generates a static exchange-polarization scattering potential was obtained by the DV $X\alpha$ method of Averill and Ellis (1973) for a nuclear geometry similar to that employed by Sink and Juras (1973). While a constant potential is used in the interstitial region, the potential in the asymptotic region consists of a polarization potential with a coefficient $\alpha =$ 46.7 au, obtained from a MRD-CI calculation by Buenker *et al* (1976) and Buenker (1992). After solution of the Schrödinger equation in each region, the scattering matrix is determined by continuity conditions at the bounding surfaces.

3. Results and discussion

The elastic differential cross sections, determined as described in section 2.1, are listed in table 1. They are also plotted in figures 1(*a*)-(*d*) together with results from the CMS calculations outlined in section 2.2. For comparison, the figures also include cross sections calculated from two independent molecular scattering theories. The data cover energy regimes above and below the electronic excitation threshold, which we take to be about 7.5 eV from our measurements.

3.1. Range I (2-7.5 eV)

Elastic scattering angular distributions obtained with electrons of 2-7.5 eV incident energy are shown in figures 1(*a*) and (*b*) together with the present CMS calculations and results from the recent SEP calculations by Jain *et al* (1991) and MSV calculations by Winstead and McKoy (1992). The figures show good accord between the present measurements and cross sections calculated from the CMS formulation. The MSV and SEP approximations at least qualitatively agree with the measured cross sections. This and previous examples in the literature (Tanaka *et al* 1990b) clearly indicate that theoretical formulations involving only local potentials with at most a non-local

Table 1. Compilation of elastic scattering cross sections. At the bottom are the integrated elastic cross sections σ_I and momentum transfer cross sections σ_M, calculated from phaseshift fits (in units of 10^{-16} cm^2).

Scattering angle θ (deg)	Incident energy (eV)										
	1	2	2.5	3	5	7.5	10	15	20	60	100
10							28.21	32.22	20.04	16.950	
20	1.835	3.655	4.470	6.991	15.81	17.49	19.24	20.11	19.20	3.536	2.0630
30	0.9723	2.470	2.732	5.271	11.66	12.56	12.83	10.23	7.094	0.4160	0.3760
40	0.4523	1.629	2.088	4.056	8.195	8.734	7.117	4.206	2.227	0.2530	0.2810
45									0.2390	0.2300	
50	0.2067	1.249	1.650	2.664	4.624	4.644	3.856	1.6390	0.6800	0.2630	0.1920
55									0.2350	0.1910	
60	0.3381	1.419	1.735	2.180	2.801	2.619	1.804	0.8150	0.4630	0.2050	0.1680
65									0.1830	0.1630	
70	0.6484	1.863	2.052	2.175	2.110	1.705	1.050	0.7240	0.4610	0.1420	0.1210
75									0.1130	0.0736	
80	0.9420	2.475	2.636	2.369	1.989	1.379	1.077	90.6300	0.4160	0.0871	0.0449
85									0.0603	0.0234	
90	0.9632	2.612	2.573	2.820	1.773	1.439	1.129	0.5970	0.2930	0.0505	0.0216
95									0.0354	0.0297	
100	0.9854	2.507	2.338	2.314	1.894	1.547	1.079	0.4910	0.1900	0.0267	0.0625
105									0.0325	0.0956	
110	0.6952	1.835	1.859	1.835	1.716	1.519	1.019	0.3760	0.1390	0.0368	0.1130
115									0.0479	0.1440	
120	0.4742	1.359	1.487	1.442	1.341	1.369	0.8480	0.3110	0.1250	0.0528	0.1160
125									0.0509	0.1060	
130	0.3256	1.222	1.422	1.431	1.387	1.176	0.6790	0.2440	0.1400	0.0438	0.0965
σ_I	8.40	26.45	28.76	34.07	45.48	43.40	39.42	30.14	23.63	7.47	6.36
σ_M	7.11	26.03	27.31	27.67	26.87	21.72	18.54	11.48	6.52	1.44	1.60

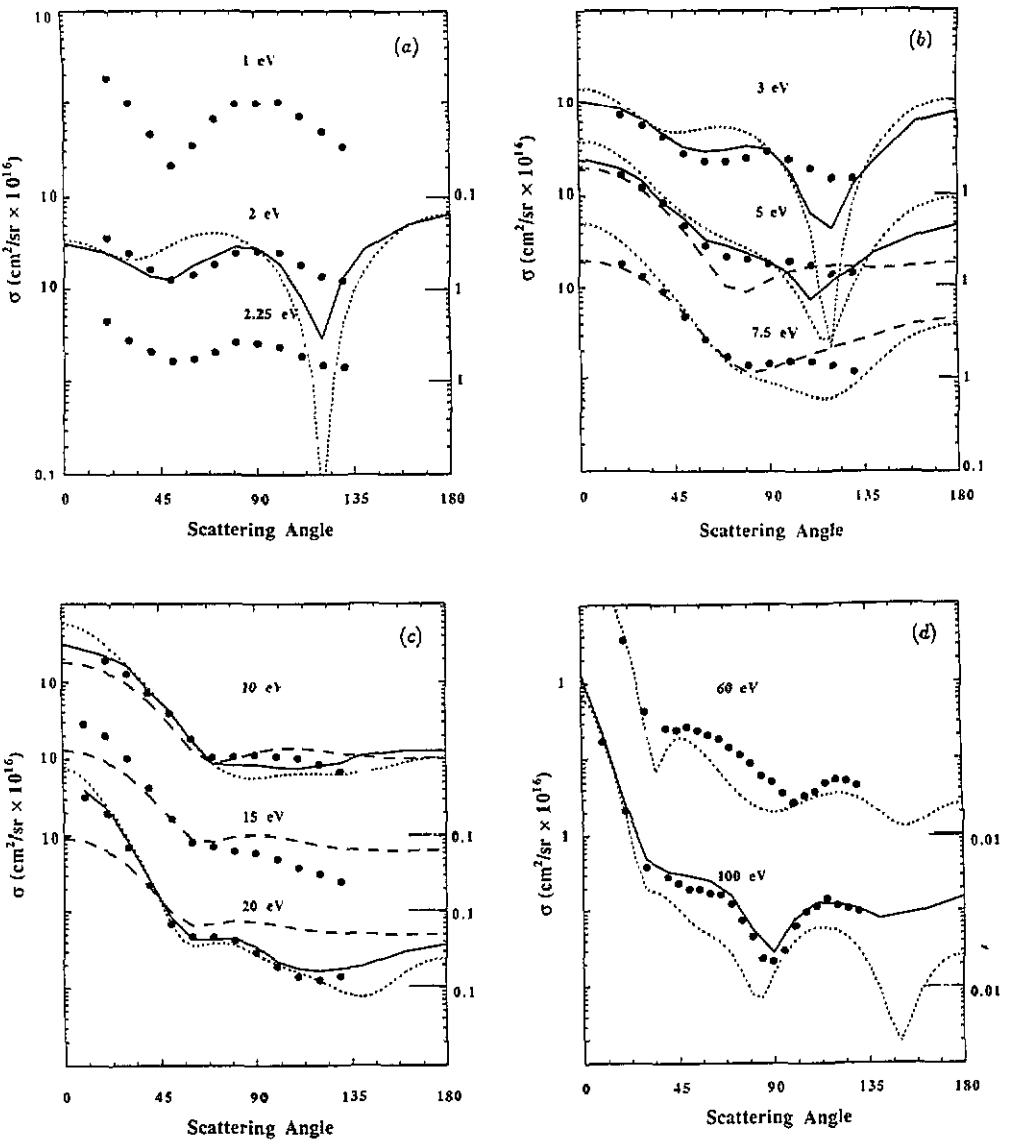

Figure 1. Elastic scattering angular distributions listed in table 1 together with some results of theory: Jain *et al* (1991), SEP (· · ·); present CMS (——); Winstead and McKoy (1992), MSV (- - - -). Also shown are results of present experiments (• • • •).

exchange potential provide a useful interpretational tool for experimental results throughout the observed energy and angular ranges. The MSV calculation, an *ab initio approach, also does quite well in this energy regime even though one defect of its* present status is the omission of polarizaton from the formulation. It will be interesting to assess its capabilities when long-range effects like polarization can be included.

A shape resonance in the t_2 scattering state found in both the CMS and SEP (Jain *et al* 1991) calculations is confirmed by a maximum near 80° in the angular distributions obtained with electrons of 1–3 eV incident energy; see figure 1(*a*). In the elastic scattering channel, temporary negative ion formation can be obscured by intrusion of

the direct scattering amplitude; thus, a study of vibrationally inelastic scattering may become necessary. However, in the present case resonance formation is quite dramatic, as observed in the elastic scattering energy distributions of figure 2, which compares excitation functions recorded at 40° and 90°. A relatively sharp peak appears only in the 90° trace at about 2–2.5 eV. The experimental resonance energy of 2–3 eV is about half the value predicted by the CMS and SEP formulations.

3.2. Range II (>7.5 eV)

Elastic scattering angular distributions for e-GeH_4 collisions for incident energies greater than the inelastic threshold are displayed in figures 1(*c*) and (*d*). The CMS and SEP calculations follow the measurements very nicely, whereas the MSV formulation appears to qualitatively reproduce experimental results for angles less than 60°, although at 10° it fares as well as the other two methods. At an impact energy of 100 eV, the angular distribution approaches that of isoelectronic Kr, except that the nearly flat shoulder at ≈60° is deeper in Kr (cf Buckman and Lohmann 1987). In this energy range, all three theoretical formulations seem to yield values in reasonable correspondence to experimental results. This observation is in accordance with the results of previous work (Tanaka *et al* 1990b), but it nonetheless seems counterintuitive. The presence of inelastic channels would normally require a complex scattering potential to satisfy detailed balance. Furthermore, a description of the problem for large scattering angles might require a non-local potential for an accurate portrayal of exchange.

3.3. Elastic integral and momentum transfer cross sections

The integral cross sections for elastic and momentum transfer, σ_I and σ_M, defined by

$$\sigma_I = 2\pi \int_0^\pi \sigma_e(\theta) \sin\theta \, d\theta \tag{1a}$$

$$\sigma_M = 2\pi \int_0^\pi \sigma_e(1-\cos\theta) \sin\theta \, d\theta \tag{1b}$$

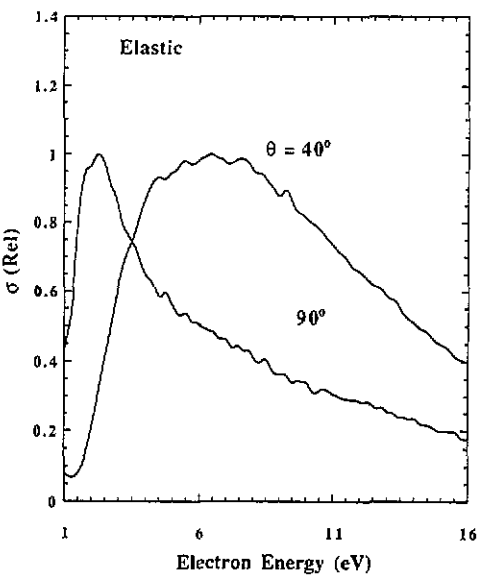

Figure 2. The energy distribution for elastic scattering at two selected scattering angles shows the presence of a shape resonance in the range 2–2.5 eV, near the local maximum of the angular distribution curve of figure 1. The ripples on both curves are noise. The two curves have been scaled to the same peak value. The peak in the 40° curve is obscured by direct scattering.

are generally required as input for modelling calculations and a reference for comparison with electron drift experiments. To carry out these integrations, the σ_e curves of figures 1(*a*)-(*d*) were extrapolated in the forward and backward directions with the help of a parametrization of the scattering amplitude f, as follows:

$$\sigma_e = |f|^2 \tag{2a}$$

$$f = \frac{1}{2ik} N(k) \left\{ \sum_{l=0}^{L} \frac{S_l(k)-1}{(2l-1)(2l+1)} P_l(\cos\theta) + C_L \right\}. \tag{2b}$$

Here k is the incident electron wavenumber, S_l is the scattering matrix, and $N(k)$ depends on the least-squares fitting procedure employed. C_L is the Thompson (1966) form of the Born approximation for higher phases beyond a cutoff L, given by

$$C_L = 2i\pi\alpha k^2 \left(\tfrac{1}{3} - \tfrac{1}{2}\sin(\tfrac{1}{2}\theta) - \sum_{l=1}^{L} \frac{P_l(\cos\theta)}{(2l+3)(2l+1)} \right). \tag{3}$$

Here, α is the polarizability. In the case of the simple phaseshift fitting as used for true spherical potentials (Andrick and Bitsch 1975) $N(k)$ would be unity and $S_l = \exp(i\delta_l)$. With only approximately spherical potentials as in the present case, $N(k)$ becomes an additional size-fitting parameter (cf Register *et al* 1980) to be determined together with phaseshifts δ_l. Obviously, this approximation changes the meaning of the phaseshifts and of α. With these modifications, equations (1)-(3) have enabled us to obtain excellent fits to experimental data for many different gases (see, e.g., Boesten and Tanaka 1991). These results follow and sometimes even anticipate theory in the expanded regions rather well. However for low L, which is limited by the number of experimental points and the intended degree of smoothing, the factor $N(k)\alpha k^2$ in equation (2) overestimates the Born correction at high impact energies, while at low energies k^2 makes the fit nearly independent of α. We have therefore performed the fits for a range of α from 25 to 55 au. At 60-100 eV, $\alpha \leqslant 35$ au had to be enforced to prevent oscillations. Fortunately, the integrated differential cross sections for these sets do not deviate much from one another (about 10-20%), and they generally reproduce the angular shape and size of the experimental results better than the theories discussed above. Integrated cross sections obtained in this way for $\alpha = 35$ au are listed at the bottom of table 1 and plotted in figure 3 together with other theoretical values and results compiled by Hayashi *et al* (1990). For energies above 7.5 eV, a second set of cross sections was computed by using a form of f valid for complex potentials. In that case equation (2*b*) is modified by letting $S_l = B_l S_l$ (Bransden 1970) where B_l contains the inelastic effects. The results of the two fittings were practically identical, and figure 3 shows that the results agree quite well with Hayashi's values. In the electron energy range of 10-12 eV, a barely discernable, broad bump appears in our experimentally determined integrated cross sections, σ_I and σ_M, coinciding with the onset of ionization (Binning and Curtiss 1990, Ruscic *et al* 1990) and the peak of ultraviolet absorption (Dillon *et al* 1985, Itoh *et al* 1986). Similarly, at 2 eV an irregularity occurs that will be discussed below.

3.4. Spectral decomposition

A vibrational EELS of GeH_4 recorded with electrons of 2.25 eV at a scattering angle of 80° is displayed in figure 4 for the loss range from −0.15 to +0.55 eV. If we consider the spectrum to be composed of a superposition of modes ν_1, ν_2, ν_3 and ν_4 at 259, 116, 262 and 104 meV (Corice *et al* 1972, Wilkinson and Wilson 1966) and include

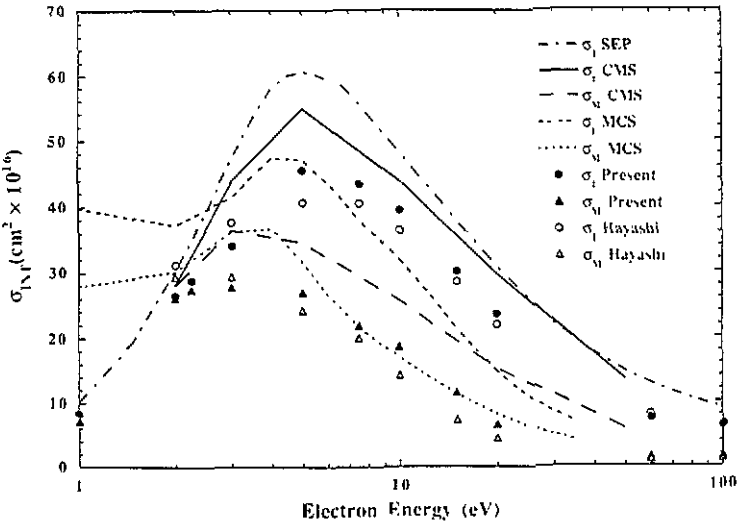

Figure 3. Energy dependence of the integrated cross sections and of total and momentum transfer, for experiments (points) and theory (full curves).

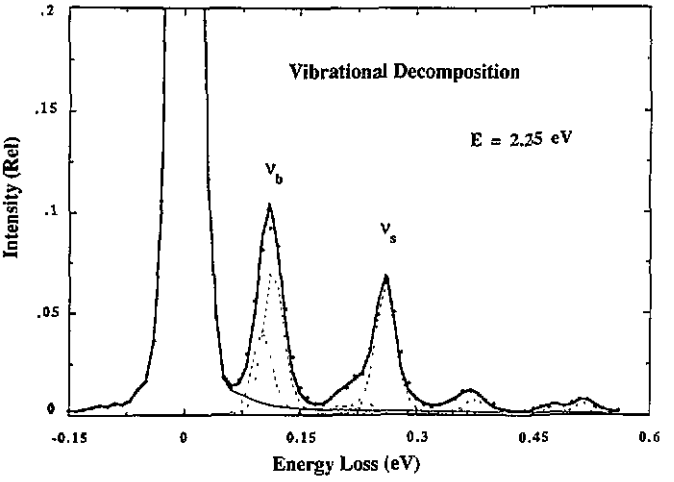

Figure 4. Spectral decomposition of an electron energy loss spectrum recorded with electrons of 2.25 eV impact energy at a scattering angle of 80°, which approximately corresponds to the peak of the 2.25 eV angular distribution of figure 1(*a*). ●, experiment; - - - - single peaks; ——, sums of single peaks.

these workers' harmonics and overtones, decomposition can be accomplished by a method described previously (Boesten *et al* 1990). First, the apparatus function is constructed from the elastic peak, including a long tail on the high-energy side that also accounts for background noise. Then a least-squares fit is applied to obtain the weights for all major combinations of peaks up to 0.55 eV so that their sum approaches the observed data as closely as possible (see figure 4). The separation between ν_1 and ν_3 is so small (0.003 eV) that any attempt to include them separately introduced

numerical instabilities. Their joint contribution is labelled ν_{13}. The final spectral assignments used in the fit and their weighting factors are listed in table 2.

2.5. Vibrational excitation

Shape resonances often reveal strong selectivity in vibrational excitation. However, because we cannot resolve overlapping vibrational modes, such an enhancement cannot be investigated definitively. Furthermore, the high degeneracy of the temporarily bound electron guarantees a decay into many vibrational modes. For $e+GeH_4$ collisions, the temporary negative ion (TNI) formed belongs to the t_2 representation in the T_d point group, and the modes into which it decays are given by its symmetric product $(t_2 \times t_2)_s = \nu_1(a_1)$, $\nu_2(e)$, $\nu_3(t_2)$, and $\nu_4(t_2)$. Hence, the two prominent compound peaks shown in figure 4, namely ν_b $(=\nu_2+\nu_4)$ and ν_s $(=\nu_1+\nu_3)$ consist entirely of modes that can be enhanced. Enhancement is shown in figure 5 by comparing two EELS recorded under dissimilar operating conditions, one off-resonance at 20 eV and 120°, while the other exhibits increased vibrational intensities near the resonance maximum 2.25 eV even though the scattering angle is also at 120°. Note that the two elastic peaks have both been normalized to unity to emphasize the enhancement. The corresponding excitation functions of ν_b and ν_s recorded at four different scattering angles are displayed in figures 6(*a*) and (*b*). Both sets confirm again that the maximum at approximately 2.2 eV becomes more prominent in excitation functions recorded at the larger scattering angles of 90° and 120°.

Angular distributions of scattered electrons for both vibrational peaks are presented in figure 7 for an impact energy near the resonance maximum. The curves have been obtained by integrating under the compound peaks of the EELS (as in figure 4) from valley to valley and performing a similar integration for the elastic peak, which is used as normalization reference. The magnitude of each point in the angular distribution depends to a large degree (±50%) on the width of the integration range, a fact that is often overlooked. Because vibrational modes ν_3 and ν_4 are triply degenerate, the angular variations of figure 7 reveal little in the way of a simple interpretation. A scattered-electron wavefunction with term symbol Φ_S in a target fixed-coordinate system

Table 2. Vibrational term symbols and weighting factors for the single peaks of the decomposition of a spectrum recorded at a scattering angle of 80° and an impact energy of 2.25 eV (cf figure 4).

Harmonics	Position (meV)	Relative weight
ν_0	0	0.9998
ν_4	102	0.0411
ν_2	116	0.0733
$2\nu_4$	204	0.0047
ν_{2+4}	218	0.0048
$2\nu_2$	232	0.0080
ν_{13}	261	0.0645
$3\nu_4$	306	0.0023
$3\nu_2$	348	0.0026
ν_{1+3+4}	363	0.0028
ν_{1+3+2}	377	0.0081
ν_{1+2+4}	477	0.0037
$2\nu_1$	518	0.0062

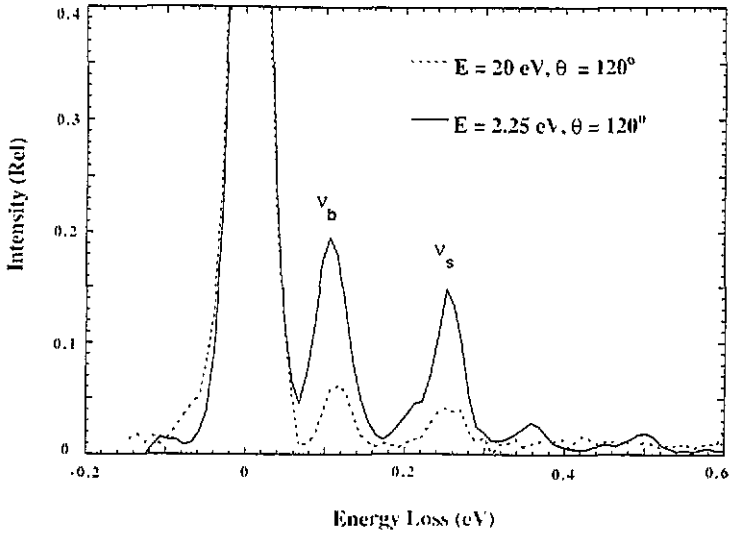

Figure 5. Comparison of two vibrational energy loss spectra. The spectrum recorded well off the resonance energy maximum is displayed as a broken curve while the full curve spectrum exhibits enhancement in both stretching and bending modes. The two traces have been scaled to obtain unit elastic cross section.

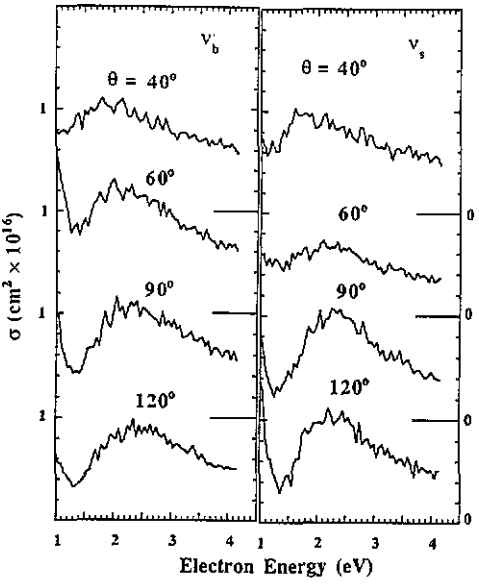

Figure 6. Excitation functions for stretching (ν_s) and bending (ν_b) vibrations for selected scattering angles. The steep increases at the left are due to instrumental effects.

is related to the TNI wavefunction with term symbol Φ_{TNI} and to the vibrational mode ν by $\Phi_S \times \nu = \Phi_{TNI}$. For $\nu = \nu_3$ or $\nu = \nu_4$, Φ_S will be superposition of irreducible representations a_1, e, t_1 and t_2. Consequently, the scattered electron wave, when written as a series of Legendre functions P_L in either the molecular or the laboratory framework, can contain terms in all L (in the similar case of CH_4 SCI, Tanaka *et al* 1983); that is, there are no symmetry relations from which one can expect a distinctive shape for angular distributions. Nevertheless, figure 7 contains a clear d-wave pattern ($l = 2$) for both peaks, suggesting that the variations in ν_s and ν_b are dominated by the behaviour

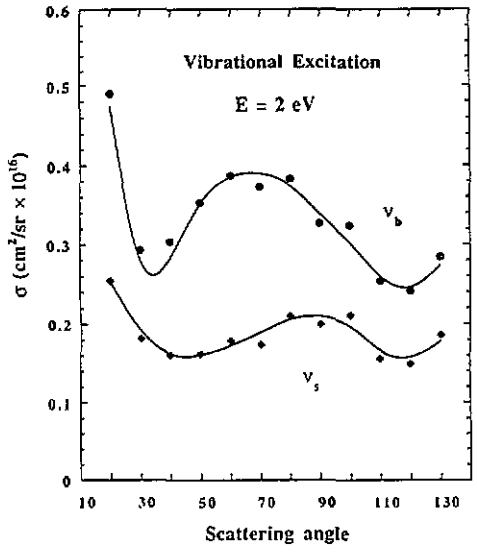

Figure 7. Angular distributions for the bending and stretching vibrational cross sections recorded with electrons of 2 eV incidence energy corresponding to the resonance peak.

of ν_1 and ν_2, respectively. This interpretation is consistent with the weights given in table 2.

2.6. Triplet state at threshold

Figure 8 shows two EELS in the electronic threshold region, scaled to counts per sweep, i.e. approximately to the same scale. The spectrum recorded at 100 eV and 10° favours singlet excitation. In fact, a measurement at 5° (not shown) revealed a small shoulder at 8.3–8.5 eV that has been assigned the $3T_2 \rightarrow 5s$ Rydberg transition, which is the lowest optically allowed state (Dillon *et al* 1985, Itoh *et al* 1986). The second spectrum, recorded for an incident energy of 20 eV at a scattering angle of 30°, favours the observation of the lowest spin-forbidden transition, $3T_2 \rightarrow 5s(^3T_2)$, which appears in figure 8 in the form of a long tail descending toward 6 eV. The corresponding tail of the 100 eV spectrum is flat at least up to 7.5 eV. The analogous $^3T_2$ state was previously

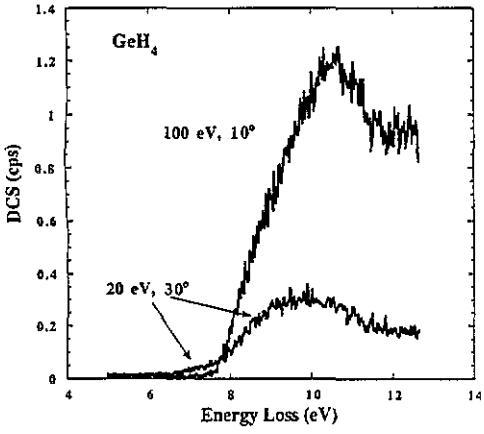

Figure 8. Electron loss spectra near the threshold of electronic excitation. The spectra are approximately normalized by conversion to counts per sweep (cps).

reported for SiH_4 (Tanaka *et al* 1990a). This state was shown in a calculation of spontaneous dissociation of SiH_4 (Tsuda *et al* 1989) to be the precursor for formation of the SiH_3 radical, confirming that the lowest triplet state in these molecules plays an important role in chemical plasma processes.

4. Conclusion

In this work we have produced an array of elastic cross sections for e-GeH_4 scattering and a selection of vibrationally inelastic cross sections to test currently applied collision theories and to provide input for future plasma studies. In the neighbourhood of 2.0 to 2.5 eV, a shape resonance has been observed in excitation functions recorded for both elastic and vibrationally inelastic channels. A number of calculations have shown that this shape resonance is related to the decay of a TNI state belonging to the t_2 representation. Because of the complex behaviour of the superimposed vibrational bands, angular distributions near the vibrational resonance peak reveal nothing definitive about the nature of the TNI. However, a similar distribution in the case of elastic scattering shows a maximum near 90° that is characteristic of decay from a TNI state with a term symbol t_2.

In addition, an exploration by EELS of the region just below the optical threshold reveals an inelastic scattering process at small impact parameter, characteristic of and undoubtedly due to excitation of the chemically important lowest triplet state.

References

Andrick D and Bitsch A 1975 *J. Phys. B: At. Mol. Phys.* **8** 393–410

Averill F W and Ellis D E 1973 *J. Chem. Phys.* **59** 6412–8

Binning R C Jr and Curtiss L A 1990 *J. Chem. Phys.* **92** 3688–92

Boesten L 1988 *Rev. Sci. Instrum.* **59** 233–7

Boesten L, Tanaka H, Kubo M, Sato H, Kimura M, Dillon M A and Spence D 1990 *J. Phys. B: At. Mol. Opt. Phys.* **23** 1905–13

Boesten L and Tanaka H 1991 *J. Phys. B: At. Mol. Opt. Phys.* **24** 821–32

—— 1992 *At. Data Nucl. Data* **52** 25–42

Bransden B H 1970 *Atomic Collision Theory* (New York: Benjamin) section 1-5

Buckman S J and Lohmann B 1987 *J. Phys. B: At. Mol. Phys.* **20** 5807–16

Buenker R J 1992 Private communication

Buenker R J, Peyerimhoff S D and Peric M 1976 *Chem. Phys. Lett.* **42** 383–9

Corice R J, Fox K and Fletcher W H 1972 *J. Mol. Spectrosc.* **41** 95–104

Dill D and Dehmer J L 1974 *J. Chem. Phys.* **61** 692–9

Dillon M A, Wang R G, Wang Z W and Spence D 1985 *J. Chem. Phys.* **82** 2909–17

Hayashi M, Kawach Y and Kozaki Y 1990 *Proc. Phys. Soc. Japan* October 3aTC4 (in Japanese) and private communication

Itoh U, Toyoshima Y and Hideo O 1986 *J. Chem. Phys.* **85** 4867–72

Jain A, Baluja K L, Di Martino V and Gianturco F A 1991 *Chem. Phys. Lett.* **183** 34–9

Kimura M and Sato H 1991 *Comment. At. Mol. Phys.* **26** 333–55

Osmundsen J F, Abele C C and Eden J G 1985 *J. Appl. Phys.* **57** 2921–30

Register D F, Trajmar S and Srivastava S K 1980 *Phys. Rev.* A **21** 1134–51

Ruscic B, Schwarz M and Berkowitz J 1990 *J. Chem. Phys.* **92** 1865–75

Sink M and Juras J 1973 *Chem. Phys. Lett.* **20** 474–7

Tanaka H, Boesten L, Kimura M, Dillon M A and Spence D 1990a *J. Chem. Phys.* **92** 2115–6

Tanaka H, Boesten L, Matsunaga D and Kudo T 1988 *J. Phys. B: At. Mol. Opt. Phys.* **21** 1255–63

Tanaka H, Boesten L, Sato H, Kimura M, Dillon M A and Spence D 1990b *J. Phys. B: At. Mol. Opt. Phys.* **23** 577–87
Tanaka H, Kubo M, Onodera N and Suzuki A 1983 *J. Phys. B: At. Mol. Phys.* **16** 2861–9
Thompson D G 1966 *Proc. R. Soc.* A **294** 160–74
Tsuda M, Oikawa S and Sato K 1989 *J. Chem. Phys.* **91** 6822–9
Wilkinson G R and Wilson M K 1966 *J. Chem. Phys.* **44** 3867–74
Winstead C and McKoy V 1992 Private communication